Revista Mexicana de Física **43**, *No. 4 (1997) 489–510*

From nuclear reactions to liquid-drop collisions

A. Menchaca-Rocha, F. Huidobro, A. Martínez-Dávalos, K. Michaelian, A. Perez, and V. Rodríguez
Instituto de Física, Universidad Nacional Autónoma de México
Apartado postal 20-364, 01000 México D.F., Mexico

N. Cârjan
CEN de Bordeaux-Gradignan, F-33170 Gradignan, France

Recibido el 10 de febrero de 1997; aceptado el 20 de marzo de 1997

Abstract. A review of the experimental and theoretical situation in coalescence and fragmentation studies of binary liquid-drop collisions is given, putting in perspective our own contributions, which include experiments with mercury and oil drops and the application of a nuclear reaction model, specifically modified by us for the macroscopic case.

Resumen. Se presenta una revisión de la situación actual de los estudios, tanto teóricos como experimentales, de colisiones binarias de gotas, poniendo en perspectiva nuestras propias contribuciones en este campo, las cuales incluyen experimentos con gotas de mercurio y de aceite, así como la aplicación de un modelo para reacciones nucleares modificado específicamente para el caso macroscópico.

PACS: 47.10+g; 03.20.+i; 25.70.-z; 47.90.+a

1. Introduction

We are engaged in establishing a bridge between fields where macroscopic liquid-drop collisions are important, and nuclear reactions modelling, particulary with those theories in which the quantal effects can, somehow, be *switched off*, allowing a direct access to the bare liquid-drop aspects. Besides providing an interesting testing-ground for those sophisticated models, this represents the opportunity of applying them to fields like meteorology and spray research, where the theoretical situation is less developed. In order to introduce the reader into this area of research, here we present a review of the current experimental and theoretical situation concerning binary liquid drop collisions, including our own findings using mercury and oil drops. These experiments have interested theoretical nuclear dynamisists to the point of establishing a fruitful collaboration with us which lead to the modification of a nuclear reaction code, developed by N. Cârjan, A. Sierk and R. Nix [1], which allows the simulation of macroscopic liquid-drop collisions. Thus, we also include a brief review of what we have learned so far in this line of research. A particular subject which recently cought our attention was the predictions [2] of nuclear fluid-dynamic simulations concerning the possibility of multifragmentation mechanisms proceeding via the formation of exotic nuclear shapes (sheets, bubbles, donuts, etc.).

Since similar predictions have also been reported for macroscopic systems [3], we carried out liquid-drop collision experiments at the relative velocities where those exotic shapes were expected to appear. The first results of that quest are also included.

This paper is organized as follows: Section 2 defines terms which are used in the rest of the text. Section 3 reviews the experimental techniques, including ours, and the results obtained for all liquids are reviewed and compared in Sect. 4. The theoretical formulations and their predictions are reviewed in Sect. 5. The conclusions are summarized in Sect. 6.

2. DEFINITIONS

Since the pioneering works of Plateau [4] and Rayleigh [5], collisions among pairs of liquid drops (henceforth simply referred to as "drops") have been investigated extensively by meteorologists (*e.g.*, Ref. 6) and atomization and spray experts (*e.g.*, Ref. 7). The evolution of this research until 1970 was thoroughly reviewed by Park [8], himself a major contributor, and until 1978 by Pruppacher and Klett [9]. More recently, the works of Podvysotsky and Shraiber [10], Ochs *et al.* [11], Ashgriz and Givi [12], Brenn and Frohn [13], Ashgriz and Poo [14], Salita [15], Jiang *et al.* [16], and Menchaca-Rocha *et al.* [17] are good examples of the continued interest in this field. Reviews of the important works written in russian may be found in the books of Vasenin *et al.* [18] and of Sterninn and Shraiber [19].

To this date, most quantitative experimental studies on "direct" collisions (those in which liquid contact is established) have been aimed at determining the boundaries between two possible outcomes: "coalescence" (one final drop) and "fragmentation" (more than one final drop) as a function of the initial collision parameters, *i.e.*, the relative velocity $\vec{v}_r$, the "impact parameter" b (measuring the centrality of the collision) and the type of liquid. Since our purpose is to further the understanding of the evolution and possible fragmentation of liquid masses formed in direct drop interactions, the term "collision" here will exclude "bouncing," a mechanism in which direct contact is prevented by the intermediate air film. Although interesting in its own right, for our aim, this gas-drainage effect will be viewed as a complication, rather than as a source of information.

The most relevant parameters determining the outcome of this type of drop collisions in air have been found [8] to be: the initial drop masses m_l and m_s, the corresponding diameters D_l and D_s, the relative speed $|\vec{v}_r|$ (or simply, v_r), the impact parameter b (Fig. 1), and the liquid's physical properties: density ρ, surface tension σ and viscosity ν. The following dimensionless parameters can thus be defined: the diameter ratio $\Delta = D_l/D_s$, the reduced impact parameter $B = b/\bar{D}$, where $\bar{D} = \frac{1}{2}(D_l + D_s)$, and the Weber number $We = \rho d v_r^2/\sigma$, where d represents a particular choice of diameter (D_l, D_s or $\bar{D}$). When dealing with asymmetric systems ($D_l \neq D_s$), we shall use the $d = D_s$ convention, adopted by most authors in this field [9]. Except for the recent work of Jiang *et al.* [16], who dealt with water and a variety of hydrocarbon compounds, little is known about the ν dependence of liquid drop collisions. We chose to compare our results (see Sect. 4) with those reported for liquids of similar viscosity so that, other factors being fixed, parameters depending explicitly on ν, such as the Reynolds number $R_e = \rho d v_r/\nu$, are not expected to vary significantly.

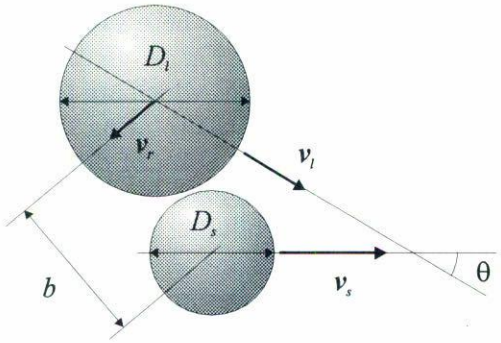

FIGURE 1. Definition of the relevant geometric collision parameters.

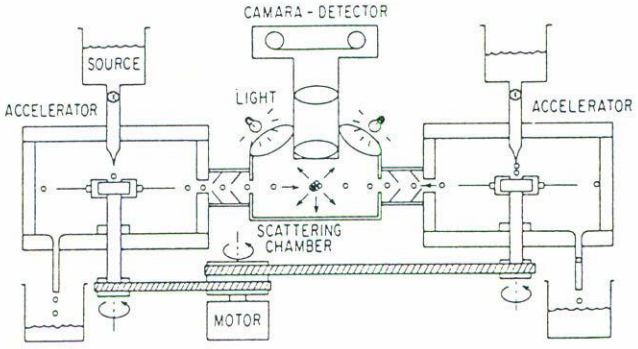

FIGURE 2. Schematic view of our high energy liquid-drop collider.

3. REVIEW OF EXPERIMENTAL METHODS

The observation of collisions between pairs of drops moving in air involves two main techniques: the controlled production of fast moving drops, and the registration of a sequence of images from which the detailed analysis of the action can be made. To this date, the most popular methods to generate drops for these type of experiments can be viewed as modern versions of the one proposed by Rayleigh [5], who produced a fairly uniform stream of equally-spaced, equal-size drops by breaking up a water jet from a capillary mechanically excited using the vibrations of a tuning fork, later replaced by an electronic device. Since then, drop collisions have been observed by aiming two of those drop streams against each other. This technique produces drops with relative speeds in the $0.1 \text{ m s}^{-1} \leq v_r \leq 10 \text{ m s}^{-1}$ range.

Faster ($v_r \leq 50 \text{ m s}^{-1}$) drops of similar sizes have been obtained by Podvysotsky and Shraiber [10] and by Menchaca-Rocha *et al.* [20] using a technique based on capillaries soldered radially to hollow cylindrical shafts. The motor-driven horizontal rotation of those shafts causes a centrifugal flow of liquid through the capillaries leading to the production of droplets in the plane of rotation. A stream of well separated liquid drops is then produced by selecting those moving in a given direction with the aid of a collimator.

The high relative velocity experiments reported here were carried out with a device of this type, which is schematically described in Fig. 2. In it, the drop-drop collisions are observed with the aid of fast stroboscopic lamps which are triggered by signals generated when a narrow handle, fixed at the bottom of the rotating shafts, points in a given direction. A variable delay unit permits the observation of different stages of the collisions. So far, our observations with this instrument have been limited to visualizations of the time evolution of the shapes assumed by colliding systems. Thus, on this respect, we shall limit ourselves to a qualitative comparison of the observed shapes with what has been predicted by both, nuclear [2] and macroscopic [3] hydrodynamic calculations.

All of the above mentioned techniques produce small ($D \leq 0.5$ mm) drops. Individual collisions involving larger (1 mm $\leq D \leq$ 5 mm) drops were observed by McTaggart-Cowan and List [21] through the use of vertical droplet accelerators combining gravitational and gas propulsion stages.

Collisions have been observed for drops approaching each other along a whole variety of relative orientations θ (see Fig. 1), from parallel ($\theta = 0°$), to antiparallel ($\theta = 180°$). Since the influence of terrestrial gravity causes all trajectories with horizontal components to have a parabolic shape, most experiments aim at reducing the local curvature to justify a straight-trajectory approximation. Under those conditions, the velocity vectors $\vec{v}_l$ and $\vec{v}_s$ define the collision plane. Thus, the initial collision parameters $\vec{v}_r$ and b are usually deduced from an analysis of images taken from a view perpendicular to that plane. Those images are obtained using fast photography, video- or cine-cameras. In the techniques used so far there is a coupling between the drop formation and the acceleration stage preventing a direct evaluation of the initial drop masses m_l and m_s. Thus the experimenters rely on values which are estimated by two methods: (a) dividing the amount of liquid collected from each droplet generator over a period of time by the number of droplets produced during the same period (*e.g.*, Ref. 14); (b) using the apparent drop-size from pre-collision images (*e.g.*, Ref. 22). The size of the collision residues (the final or "residual" drops), have also been obtained from photographic images (*e.g.*, Ref. 21).

The accuracy of these measurements demands on a number of conditions, difficult to fulfill. In the case of m_l and m_s, method (a) requires that the mass spectrum of the droplets has a narrow distribution, while in method (b) the distance from the droplet streams to the image-taking device should not change from drop to drop. Since the precise instant at which the initial drops come into contact is seldomly registered, the determination of B is based on the assumption [8] that the drop trajectories are smooth and that the line of sight of the camera is strictly perpendicular to the collision plane. A problem common to small v_r measurements is that the droplets are often observed to approach each other slowly while falling in air at large speeds. In those conditions, not only their motion occurs in turbulent air, but the interaction between the droplets' wakes introduces distortions on the trajectories [11].

Important progress has been made to understand and reduce these sources of uncertainty in the determination of initial conditions. Examples of this are the works of Park and Crosby [23] and Brenn and Frohn [13] concerning the influence of the liquid flow-rate and the capillary oscillation frequency on the width of mass distributions of Poo and Ashgriz [24] on the influence of air-drag on the drop stream, of Vassallo and

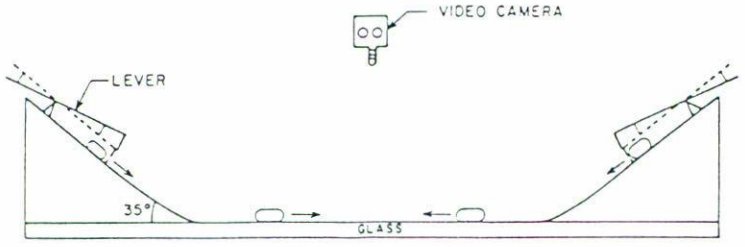

FIGURE 3. Schematic view of the low energy liquid-drop collider.

Ashgriz [25] on the formation of satellite drops in the breaking up of the liquid jet, and of Adam, Lindbland, and Hendricks [26] who proposed a modification to the Rayleigh method in which the influence of the ambient air dragged along by the droplet streams is eliminated by electrostatically selecting out of the streams the individual droplet pairs to be observed. So far, however, little has been done to reduce the uncertainties associated with the determination of final parameters where, for example, the size of drops just after the collision is difficult to estimate from photographic plates since, in general, they are oscillating and rapidly moving away from the focal plane of the image-taking device. To our knowledge, collecting the individual residues for a direct evaluation of their size had not been attempted before our work.

Some of the problems just described would be solved if a technique could be developed in which: (a) the mass of all droplets (initial and final) could be measured accurately, and (b) the position of all droplets could be followed in space as a function of time. One such technique is now described which is based on observing the interactions of mercury drops moving along a specially treated horizontal glass surface. We have built a liquid-drop collider to observe the interactions of mercury drops moving along a flat, horizontal, glass surface, in which the drag induced by wetting is minimized by a roughening procedure which greatly reduced the mercury-glass contact (Fig. 3). As described in detail elsewhere [27], this procedure results in a five-fold gain in the mobility of the mercury drops. Collision experiments involving mercury drops moving on solid surfaces have also been reported by Salita [15]. However, this interesting work was limited to 30 collisions, allowing only a rough determination of the coalescence-fragmentation transition, and giving no quantitative details about the fragmentation process.

In our low energy liquid drop collider the initial drops of pre-determined masses m_l and m_s, are "accelerated" to velocities $\vec{v}_l$ and $\vec{v}_s$ with the aid of plastic ramps fixed on two extremes of the glass surface (Fig. 3). A groove on each ramp surface guides the drops down the slopes and smoothly into parallel trajectories separated by an impact parameter b. In this way, the outcome of the drop collisions can be studied as a function of b, $\vec{v}_r$ and Δ. The position *vs.* time information, needed to determine the initial parameters $\bar{v}_r$ and b, as well as the speed v_i and direction of motion θ_i of each final drop i, is obtained by recording the action with a fast-shutter-speed (1/10 000 s) video system having a 30 frames/s recording frequency. The final number of drops, the "multiplicity" (N_f), is measured by counting the number of residual droplets; however, since secondary scattering (often leading to coalescence) among the primary fragments is not infrequent, a "primary" multiplicity (N_p) can also be extracted by replaying the video images. The

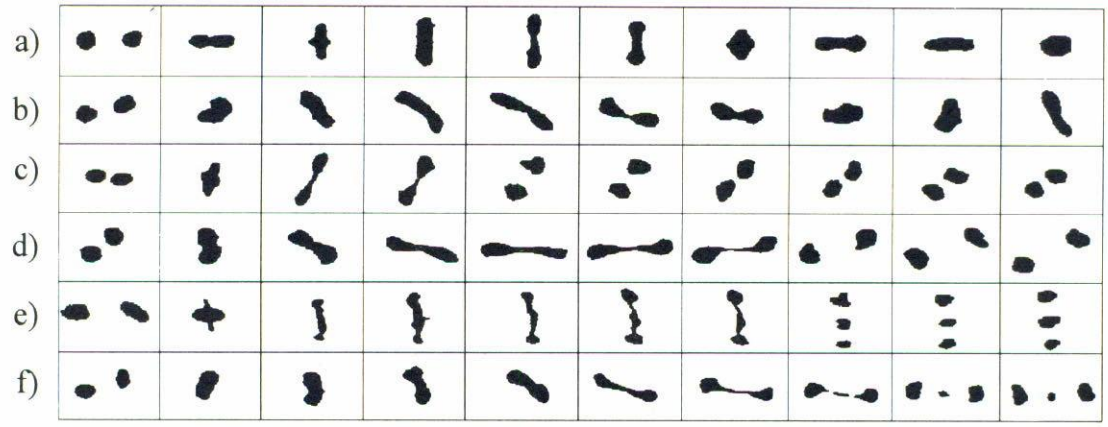

FIGURE 4. Time evolution of symmetric mercury drop collisions. Central coalescence in (a) and peripheral coalescence (b). Small-B two and three body central fragmentation in (c) and (e), respectively. Large-B two and three body peripheral fragmentation in (d) and (f), respectively. The drops move initially against each other in the horizontal direction, the time runs from left to right with $\Delta t = 1/30$ s from frame to frame. The $[We, B]$ values corresponding to each time sequence are: [48.9, 0.02] for (a), [15.2, 0.58] for (b), [44.7, 0.1] for (c), [25.0, 0.82] for (d), [83.6, 0.01] for (e), and [34.8, 0.62] for (f).

initial and final masses are measured with a 0.1 mg precision analytic scale. For technical reasons [27], the gotatron is limited to observe collisions of mercury drops having masses and velocities in the range 0.2 g $\leq m_{l,s} \leq$ 2.0 g, and 5 cm s^{-1} $\leq v_{l,s} \leq$ 50 cm s^{-1}, respectively. The action of every drop-collision experiment lasts, typically, 1 s (*i.e.*, 30 frames). Therefore our data is based on the analysis of approximately 30 000 frames. The image information on each frame consists of 620 000 color pixels. For simplicity, in the present study this volume of information is reduced to the drop contours on each frame, using standard image processing techniques. Figure 4 shows typical image sequences taken during coalescence, and fragmentation collisions. More details about the drop "acceleration" procedure used may be found elsewhere [27].

The main advantages of the gotatron are: (a) it decouples the drop formation and the acceleration stages, permitting a precise measurement of the initial masses before acceleration; (b) because the motion is restricted to the horizontal plane, the final drops travel a finite distance along the glass surface and then stop, allowing us to collect them and weigh them individually; (c) restricting the motion to a plane eliminates the ambiguities introduced by out-of plane components in three dimentional motion, allowing more accurate determinations of the collision parameters from images taken from a fixed view; (d) the lack of vertical motion minimizes the velocity of the drops relative to air which, as mentioned before, is particularly important for small We measurements, and (e) compared with other liquids (water, glycerin, etc.), our larger D ($\approx$ 5 mm) and higher density-to-surface tension ($\rho/\sigma = 0.03$) drops allow observations at lower v_r values for the same We number, further reducing the influence of the ambient gas. As we shall see, measurements with larger drops also allow us to test the generality of the scaling variables used in this field.

The main disadvantages of this instrument are: (a) the mercury-glass interaction affects the drops' motion, (b) these, relatively large, drops oscillate around a non-spherical mean shape, (c) the drops "roll" [27] (rather than slide) along the glass surface, and (d) compared to collisions among free-moving drops where the dynamics of the most central (small B) ones involve important out-of-plane components, in our case those components are strongly damped. In spite of these complications, the next Section shows how the quantitative features we observe for mercury drops remain similar to those reported for collisions between free-moving drops.

4. RESULTS

The measurements presented here involve collisions of liquid drops in two rather different regimes, low energies, where coalescence (fusion) and few-body fragmentation compete, and higher energies, were most collisions produce a large number of residues (multifragmentation). Thus the results will be presented and discussed separately in the next two subsections.

4.1. LOW ENERGY MEASUREMENTS

The data corresponding to mercury drops result from the analysis of 1000 collisions, half of them symmetric ($m_l = m_s = 1$ g) and the rest for asymmetric ($m_l = 1.5$ g, $m_s = 0.5$ g) pairs. Since these drops are non-spherical, we shall use the horizontally-projected diameter to allow the comparison with collision data from spherical drops. This corresponds to $D = 4.9$, 6.5, 8.1 mm for $m = 0.5$, 1.0, 1.5 g, respectively [27]. Hence, for asymmetric systems we shall use $\Delta = 1.65$. The collisions were measured within the 20 cm s^{-1} $\leq v_r \leq$ 90 cm s^{-1} range. No systematic $v_r < 20$ cm s^{-1} measurements were done since that region is dominated by permanent coalescence. The maximum of $v_r = 90$ cm s^{-1} corresponds to the operational upper limit of the collider [27]. Some of the figures in this Section contain theoretical predictions which will be presented in Sect. 5.

Figures 4a–4f illustrate the time evolution (from left to right) of typical coalescence [rows (a) and (b)], two-body [rows (c) and (d)] and three-body [rows (e) and (f)] fragmentation, $\Delta = 1$, collisions. Rows (a), (c), and (e) correspond to central ($B \approx 0$) and (b), (d), and (f) to peripheral ($B \approx 1$) interactions. In our experimental situation, where aerodynamic effects (such as bouncing) are small, below certain critical We all central collisions lead to coalescence. The top sequence [row (a)] is an example of a coalescence interaction observed just below that limit. Upon contact (between frames 1 and 2) a neck-like structure is formed. Eventually (third frame), incompressibility forces a flow perpendicular to the incident direction. This flow forms cylindrical shapes. Below the limiting We condition, those cylinders develop an intermediate neck (fifth frame) strong enough to support the flow-driven stretching. The subsequent evolution (frames 6 and beyond) show a damping oscillatory motion with maximal elongations alternating between being parallel and perpendicular to the incident direction. As shown in row (b), off-center coalescence interactions also form stretching cylinders, now rotating (frames

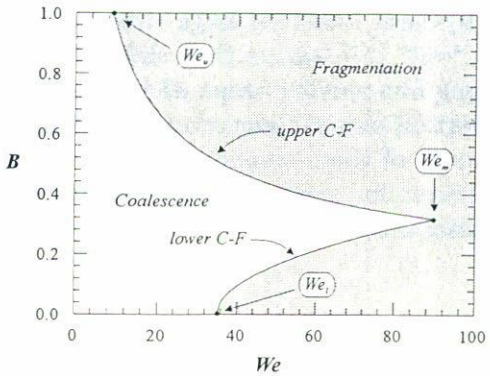

FIGURE 5. Schematic representation of the important boundaries and critical points defining the limits of coalescence in the B *vs.* We plane.

3 and 4), eventually developing intermediate necks (fifth frame) which, below a certain B-dependent limiting We, are strong enough to support the inertial pull of the outer liquid-masses. After reaching a maximal stretching stage (between frames 5 and 6), the shape evolution consists of a combination of (damping) vibrational and rotational motions. The initial stages of $B \approx 0$ two-body [row (c)] and three-body [row (e)] fragmentation are similar to the lower We central coalescence interactions [see row (a)], with an initial perpendicular flow, forming stretched cylinders on which now one or two (or more) unstable necks evolve, eventually leading to the formation of two, three (or more) residues. Peripheral fragmentation [rows (d) and (f)] also evolve initially in a way which is qualitatively similar to the lower We case [row (b)], except that stretching now leads to the formation of one or two (or more) unstable necks which break up into two, three (or more) residues.

The time sequences shown in Fig. 4 are qualitatively similar to what has been reported (*e.g.*, [8]) for collisions of drops moving in free space in the same We regime, with the existence of critical limiting We values for both peripheral and central interactions and the formation of stretched cylindrical configurations which, depending on B and We, can break into two, three or more fragments. As mentioned before, the most important difference occurs for $B \approx 0$ collisions [rows (c) and (e)]. In free space, the outward flow (along the contact plane) leads to the formation of disk-like structures which eventually collapse forming the unstable cylinders [28]. Thus, the residues are emitted in a direction parallel to the incident one. In our case, however, the initial flow is constrained by gravity to the horizontal plane, thus forming the unstable cylindrical configurations in the initial outward-flow stage (not in the subsequent collapse). Consequently, our $B \approx 0$ fragmentation residues are emitted in a direction perpendicular (instead of parallel) to the incident direction.

The existence of a well defined boundary between coalescence and fragmentation (the limiting We) was first established by Adam *et al.* in 1968 [26]. As shown schematically in Fig. 5, in the We *vs.* B plane this C-F boundary begins at a critical We_u value, below which all collisions (in which liquid contact is stablished) lead to permanent coalescence.

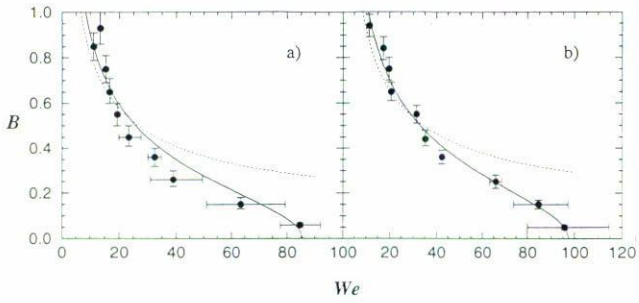

FIGURE 6. The C-F boundary extracted from the $\Delta = 1$ (a) and $\Delta = 1.65$ (b) mercury-drop data. The curves represent the general behavior observed for collisions in space (dashed) and how we expect it to be affected by "rolling" (solid).

Beyond We_u, the C-F boundary typically adopts a $B_c \propto We^{-1/2}$ dependence, which we shall call the "upper" C-F branch. Some experiments indicate that a second critical value We_l appears at $B = 0$, beyond which fragmentation also occurs. As We is increased, this fragmentation mode extend towards non-zero impact parameters following a (not well established) increasing function of We, which will be called the "lower" C-F branch. When observed, this branch is reported to merge into the upper branch at $B \approx 0.2$. Such crossing defines another important critical value, We_m, beyond which coalescence ceases to be observed.

Since, as explained in Sect. 5, the mechanisms determining the upper and lower C-F branches are generally thought to be different, the present discussion will be made separately for the upper and lower C-F branches. The C-F boundary extracted from our mercury-drop experiments is shown in Figs. 6a and 6b, for the $\Delta = 1$ and $\Delta = 1.65$ data, respectively.

The B *vs.* We data sets from other authors are shown in Figs. 7a–7f and 8a–8d, for symmetric and asymmetric collisions, respectively. As can be observed, there is a qualitative similarity between them, showing a typical

$$B_c = We_u / We^{1/2} \tag{1}$$

dependence (solid curves), where We_u is the value of We at $B_c = 1$. The common shape of the upper C-F branch allows us to reduce the comparison to the relative values of one parameter, We_u, obtained from a fit to the data using Eq. (1). In Sect. 7 we see how the deviation from this systematics found in the low B (high We) region of the mercury data can be understood as due to "rolling" (solid curves in Fig. 6). Note that, at $B = 1$, both predictions (dashed and solid curves) are very similar. In Fig. 9a we plot the We_u values obtained for all the $\Delta = 1$ data as a function of D, while in Fig. 9b we show how that parameter varies with Δ. The solid lines in these figures are, in Fig. 9a, the mean experimental value and in Fig. 9b the prediction of the model [22] which provides the best description (see Sect. 5).

Figures 9a and 9b, show that the We_u values measured from mercury-drop experiments are consistent with those found for other liquids using standard experimental techniques. Although there is an important dispersion, the data also indicates the ad-

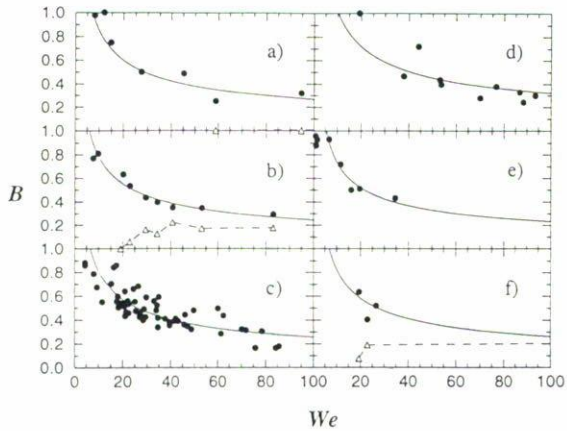

FIGURE 7. Comparison of available B *vs.* We, $\Delta = 1$, measurements. In (a) the data of Adam *et al.* [26] for $D = 120$ and 600 μm water drops; in (b) the $D = 200$–1000 μm the data deduced (see Sect. 6.1) from the water data Ashgriz and Poo [14]; in (c) the $D = 300$–1500 μm data of Ref. 22; in (d) the $D = 72$, 100, 160 and 200 μm propanol data of Ref. 13; in (e) the $D = 300$ μm water data of Ref. 16; and in (f) the $D = 200$ and 700 μm data deduced from the water measurements of Park [8]. The •'s correspond to upper C-F data, while the △'s are lower C-F data. The solid curves represent a $B_u = We_u/We^{1/2}$ fit to the •'s, leaving We_u as a free parameter. The dashed lines are drawn through the △'s to guide the eye.

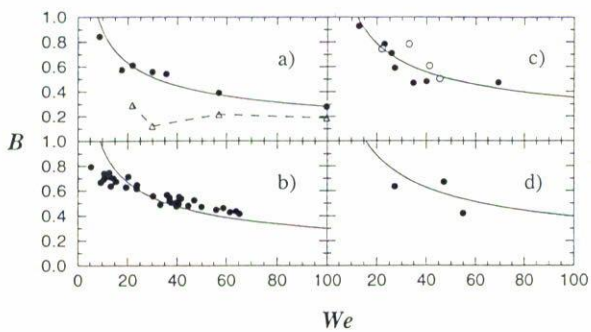

FIGURE 8. Comparison of available B *vs.* We, $\Delta > 1$, (all water) measurements. In (a) $\Delta = 1.33$ data deduced (see Sect. 6.1) from the measurements of Ashgriz and Poo [14]; in (b) the $\Delta = 1.75$ data of Brazier-Smith *et al.* [22]; in (c) the $\Delta = 2$ data deduced from the data of Ashgriz and Poo [14], (full symbols) and the data of Park [8], (empty symbols); and in (d) the $\Delta = 3$ data of Park [8]. The •'s and ○'s correspond to upper C-F data, while the △'s are lower C-F data. The solid curves show the fit to the •'s using Eq. (1) leaving We_u as a free parameter. The dashed lines are drawn through the △'s to guide the eye.

equacy of We as a scaling variable for $\Delta = 1$ collisions. Note that our mercury data allowed us to extend this verification almost two orders of magnitude in D.

As mentioned before, in central collisions a second critical value We_l defines the limit for $B = 0$ coalescence. From that point in the B *vs.* We plane fragmentation extends to the small (non-zero) B region following an (as yet undefined) direct function of We: the

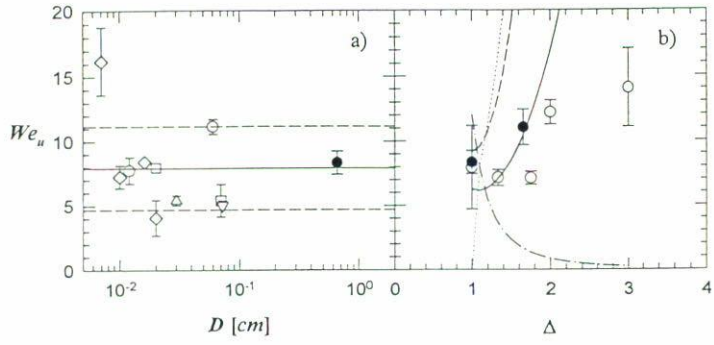

FIGURE 9. Diameter (a) and asymmetry (b) dependence of We_u obtained from the data in Figs. 6, 7, and 8. In (a) the $\Delta = 1$ data corresponds to cases for which the drop diameters are known, namely: the water data of Adam *et al.* [26] (○), the propanol data of Brenn and Frohn [13] (◇), the data of Park [8] (□), the water data of Jiang *et al.* [16] (△), the water data of Brazier-Smith *et al.* [22] (▽), and the present mercury data (•). The horizontal lines represent the mean experimental value (solid) and its incertainties (dashed). In (b) the two $\Delta = 1$ values correspond to the mean experimental value (○), and our mercury data point •, the $\Delta = 1.33$ corresponds to data by Ashgriz and Poo [14], the $\Delta = 1.65$ is our mercury data point, $\Delta = 1.75$ is data from Brazier-Smith *et al.* [22], the $\Delta = 2$ is an average from the corresponding data of Park (1970) and of Ashgriz and Poo [14], and the $\Delta = 3$ is data from Park [8]. The lines represent the predictions of models by Brazier-Smith *et al.* [22] (solid), by Schmidt and Lutz [35] (dashed), by Park [8] (dotted), and by Arkhipov *et al.* [31] (dot-dashed).

lower C-F branch. Thus, the point where the upper and lower C-F branches cross define We_m, the highest We for coalescence (independent of B).

Although our experimental method introduces a distorting effect in the low B region which prevents us from drawing conclusions on this aspects from the present mercury drop data, we would like to comment briefly on the situation concerning the available data from collisions in space.

First, the values of the zero-impact-parameter limit We_l vary widely. For example, in the case of $\Delta = 1$ water systems, Ashgriz and Poo [14], as well as Park [8], report $We_l \leq 20$, while Adam *et al.* [26] found values in the $We_l = 60$–100 range.

Secondly, the situation concerning We_m is also intriguing. The only measurements showing this limit, those of Adam *et al.* [26], yield $We_m \approx 100$ for small ($D = 120$ μm) and $We_m \approx 450$ for larger ($D = 600$ μm) drops. This result would indicate that, contrary to intuition, the temporary system formed by two small drops is less stable that formed by bigger ones. It should be added that no other measurements, including those of Brenn and Frohn [13], reaching $We \approx 480$, for $D = 160$ μm propanol drops, have established a high We limit for coalescence. Clearly this situation deserves further investigation.

Among the other drop-collision parameters which have received some attention is the residue's mass, and multiplicity (N_p), distributions. The N_p-dependence of the (We- and B-integrated) frequency distribution of the residues' mass m_i (normalized to the total mass of the system $m_t = m_l + m_s$) from mercury drop collisions is shown in Figs. 10a–10d and Figs. 10e–10h for $\Delta = 1$ and $\Delta = 1.65$, respectively. In both cases, fragmentation is found to produce two masses similar to the initial ones (the "quasi-

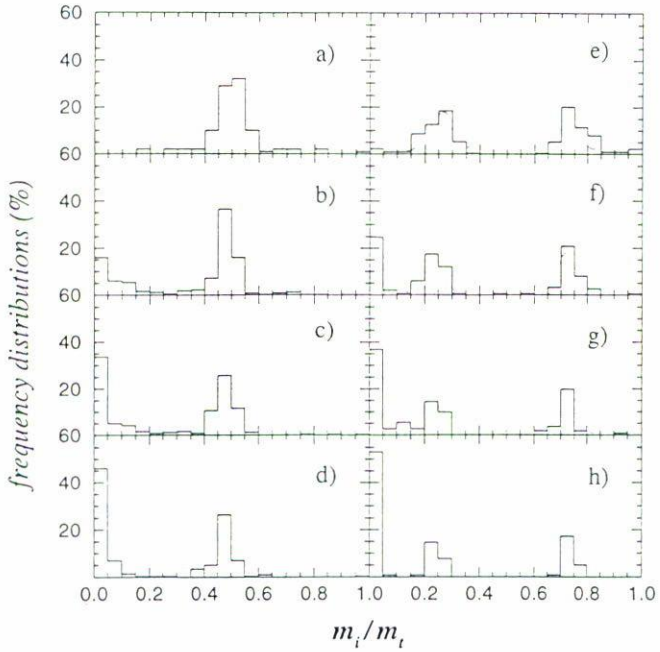

FIGURE 10. Fractional-mass frequency distributions for $\Delta = 1$ (left column) and $\Delta = 1.65$ (right column) systems, with $N_p = 2$, 3, 4 and ≥ 5 in rows (a), (e); (b), (f); (c), (g); and (d), (h), respectively.

initial" residues), accompanied by tiny ("satellite") drops. This figure shows that the increment in multiplicity is linked to an increasing number of satellite drops, but seems to have little impact in reducing the gap between the different mass groups.

This behavior can be compared with measurements for $\Delta > 1$ by List *et al.* [29], McTaggart-Cowan and List [21], and Bradley and Stow [30] for water drops and by Arkhipov *et al.* [31] for water-glycerine solutions. As in our case (*e.g.*, compare Figs. 10e–10h with Fig. 6 of List *et al.* [29] and Fig. 1 of Bradley and Stow [30]), the fragmentation of asymmetric systems is characterized by a three-peaked residue-mass distribution, two of the groups corresponding to the quasi-initial masses, and the third group to smaller satellite drops.

4.2. HIGH ENERGY MEASUREMENTS

Concerning our search for exotic shapes formed in the collisions of liquid drops at higher We's, Fig. 11 illustrates the kind of pictures we observe. For central collisions, once the two drops touch, incompressibility leads to an ejection ("squeeze-out") of liquid along the contact plane forming pseudo-toroidal shapes which, when observed on an inclined plane, always seem to have a thin liquid membrane filling their central region. Radial flow induces a rapid increase in the radius of this pseudo-torus, reducing its cross-section and transforming the system into a thin disc having a somewhat thicker rim. This bordering rim eventually develops a fingering ("mexican hat") instability

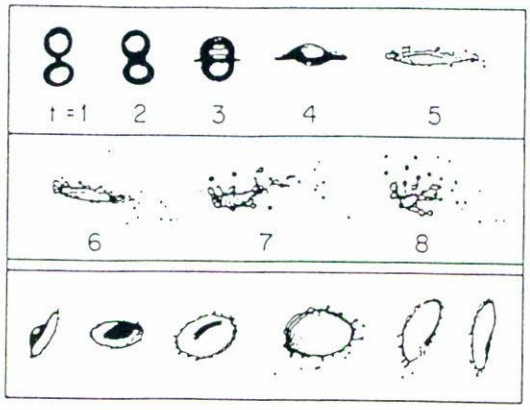

FIGURE 11. Typical images from fragmentation water drop collision at $We \approx 150$. The top two rows show the time evolution of one collision. The bottom row shows different views of the "mexican hat" instability (see text).

which initiates the fragmentation process. When compared with the macroscopic fluid-dynamic predictions (see Fig. 19 of Ref. 3), we see that an important difference lies in the central liquid film, which the models predict to breakup in the early stages leaving a true torus which eventually fragments through some form of Rayleigh instability. The experiments indicate that those central films live longer than the rapidly expanding tori. This difference with the prediction may be related to the approximate way in which surface tension is treated in the model. That problem may also be present in nuclear fluid-dynamic calculations, which have a similar approach to surface tension. Recently, Moretto *et al.* [2] described the fragmentation of both sharp (as in macroscopic systems) and diffuse (as in nuclear systems) surface liquid sheet as due to a geometrical instability which would tend to reduce the high surface-energy by breaking into a number of cylinders which, in turn, break into spherical drops via Rayleigh instabilities. Tori ("donuts") are also described by Moretto *et al.* [2] as unstable shapes which are independent from sheets. Our observation with macroscopic liquids indicates that true tori (*i.e.*, not having a thin internal membrane) should be very rare since, among thousands of collisions we have not identified a single one. Instead, most events show the formation of thin liquid sheets held by a thicker border. Like soap films held by a bubble-making rings, those liquid films are fairly stable, fragmenting only after their bordering frame does. The dynamical breaking of this frame is also somewhat different from the Rayleigh-type instability of a toroidal liquid mass.

5. COALESCENCE-FRAGMENTATION (C-F) BOUNDARY MODELS

The stability of systems formed when two drops collide has been the subject of extensive theoretical investigation. The general interest and sophistication of the models vary enormously depending on the field of application. In meteorology, for example, the concern is to understand the limiting conditions for permanent coalescence, *i.e.*, the C-F boundary, using simple mechanical arguments. Atomization and spray experts, more

concerned with fragmentation, rely on fluid-dynamic models to understand their data. At the microscopic scale, molecular and nuclear physicists deal with collective aspects of clusters and nuclei as if they were drops, having developed sophisticated quantal and semi-quantal models which include important fluid-dynamic components. As we shall see, in one of those models the quantal and Coulomb effects can be cleanly "switched off" allowing us to compare their predictions with experimental data from the macroscopic domain through the appropriate scaling. This Section contains a brief review of those theories and their predictions.

5.1. THE UPPER C-F BRANCH

Since, as we shall see, most models predict that upper C-F branch should follow (or nearly follow) the $1/We^{1/2}$ dependence observed experimentally (Figs. 7 and 8), the goodness of the predictions in this respect can be better judged by the ability of each theory to reproduce the mean $\overline{We}_u = 7.19 \pm 3.24$ extracted from Fig. 9a. Another important aspect to be considered is the Δ dependence predicted by the models which is compared with the corresponding data in Fig. 9b.

5.1.1. Neck vs. bulk-motion models

The upper C-F branch for symmetrical systems was first interpreted by Adam *et al.* [26] as due to a rotational instability. They observed that, before disruption, large B-value systems assume a rotating dumb-bell shape, *i.e.*, two large masses joined by an intermediate neck, rotating about the center of mass. Based on this, they made an estimate for the onset of disruption at $B = 1$ by assuming that all the kinetic energy transforms into rotational energy. Under those conditions the stability of the dumb-bell was made to depend on whether the neck had sufficient strength to stand the centrifugal pull of the two (equal) external masses. Using an empirical critical neck shape, their prediction [26] corresponds to $We_u(\Delta = 1) = 2.1$, a factor of approximately 4 below the mean experimental value (Fig. 9).

Park [8] modified the model to predict $B \leq 1$, and $\Delta \geq 1$, values, by introducing an idealized B-dependent neck dimension and assuming angular momentum, instead of energy-conservation. The B *vs.* We dependence predicted by this model can be calculated using the expressions

$$B_u = \left(\frac{12c}{\pi We}\right)^{1/2} \left[\frac{(1+\Delta^3)(1+\Delta^5)}{5\Delta^3(1+\Delta)} + \frac{(1+\Delta)}{2}\right], \tag{2}$$

where $c(B)$ is the neck variable

$$c = \left\{4\Delta^2 - \left[B(1+\Delta) + \frac{(1-\Delta)}{B}\right]^2\right\}^{1/4}$$

These equations underestimate the data by predicting $We_u = 0$ for symmetric systems (Fig. 9a), while, as most other models, yielding a Δ dependence for We_u (Fig. 9b) which increases more rapidly that observed.

More recently Ashgriz and Poo [14], arguing that separation occurs much earlier than the development of any significant rotation, rejected the rotational limitation concept, proposing instead a model in which a fraction of the linear kinetic energy, termed "stretching energy," is required to balance the surface attraction of a critical neck. Thus, as proposed by Adam *et al.* [26], large B disruption is said to occur whenever the sum of the linear kinetic energies of the non-overlaping masses and of the overlapping masses weighted by B^2, exceeds the surface energy of the neck, approximated by a cylinder having the length $l = D(1 - B)$ and a mass equal to that contained in the projected overlapping volumes. This model results in high order polynomials relating B to We which, for $\Delta = 1$ can be reduced to

$$We(\Delta = 1) = 8[3(1 - B)^3(1 - 2B)]^{1/2}. \tag{3}$$

Since, $B = 1$ implies no volume-overlap (hence, no neck), contrary to the experimental observations (Figs. 9a and 9b) this formulation predicts $We_u = 0$ for all Δ values [see Eq. (32) of Ref. 14].

5.1.2. Energy balance model

Brazier-Smith *et al.* [22] proposed two models to interpret the upper C-F branch. One of them avoids complicated shape parameterizations by proposing that the system would be unstable when the rotational energy exceeds the surface energy necessary to form two (spherical) droplets out of the (spherical) coalesced system. This lead to the expression

$$B_u = \left[\frac{4.8f(\Delta)}{We}\right]^{1/2}, \tag{4}$$

where

$$f(\Delta) = \frac{\left[1 + \Delta^2 - (1 + \Delta^3)^{2/3}\right](1 + \Delta^3)^{11/3}}{\Delta^6(1 + \Delta)^2}$$

is a function which varies from 1.3 for $\Delta = 1$ to 2.2 for $\Delta = 1.65$. This model [22] has been used extensively [8] as it provides a reasonable fit to most of the available upper C-F branch data, predicting a $We_u = 6.29$ for symmetric ($\Delta = 1$) systems, in good agreement with the experimental observations (see Fig. 9a). The corresponding prediction for the Δ dependence of We_u, being more rapid that observed (Fig. 9b), is the one that provides the best fit for this kind of data, failing only at the highest Δ values.

5.1.3. Shape evolution models

The second model in Brazier-Smith's *et al.* work [22] is based on the similarity between the equilibrium configurations of a rotating liquid drop near the limiting angular momentum L_c for symmetric breakup, and the last stages of a large B collision. This approach represents a conceptual improvement over the above-mentioned models because it takes into account, not only the change in surface energy, but also the change in moment of

inertia between the equivalent sphere and the limiting dumb-bell configurations. The Brazier-Smith *et al.* [22] estimate corresponds to

$$B_u = \left[\frac{\zeta(\Delta^3+1)^{13/6}}{\Delta^3(1+\Delta)We^{1/2}}\right], \tag{5}$$

with $\zeta = 4.26$. Unfortunately, this prediction grossly overestimates the experimental values, yielding $We_u(\Delta = 1) = 91.7$ with a Δ dependence (not shown) more rapid than observed. These authors [22] also noted that their predicted L_c values are factors of 3.5 larger than the experimental values.

This connection between colliding drops and the equilibrium configurations of a rotating mass was studied in more detail by Cohen *et al.* [32], (see also Ref. 33) who calculated the total (surface+electric+rotational) potential energy surfaces to determine the saddle point for the symmetric "fissioning" of an electrically charged rotating drop. When applied to uncharged masses, the Cohen *et al.* [32] theory yields a $\zeta = 2.78$ to be used in Eq. (3), corresponding to $We_u(\Delta = 1) = 4.43$. This value, being 35% below the experimental one (Fig. 9) is clearly in better agreement than what Brazier-Smith *et al.* [22] estimated within the same theoretical framework. Still, the L_c values predicted by the Cohen *et al.* [32] theory are, typically, a factor of 2 larger than the experimental observations (Fig. 9). On this problem, our group [17] used a three-dimension surface potential model developed more recently by Blocki and Swiatecki [34] to search for the L values in which the energy pocket disappears. Although this new approach still gave larger than expected L_c's, we have shown [17] that the overestimation can be reduced by introducing, in a simplified way, dynamical effects. An interesting way of doing so was proposed by Schmidt and Lutz [35]. Based on the Cohen *et al.* [32] saddle point calculations, they argue that the complex deformations observed in colliding systems result in shallow potential multidimensional energy surfaces. Thus disruption is said to set in when the centrifugal+surface energy barrier located at the saddle is overcome by the total collective energy of the equivalent spherical complex. Schmidt and Lutz [35] also extended this type of calculations to predict the upper C-F branch. In our notation, their [35] result can be written as

$$B_u = \left[\frac{24}{5}\frac{(\Delta^3+1)^{13/3}}{\Delta^6(\Delta+1)}\frac{Y_c}{We}\right], \tag{6}$$

where $Y_c = 0.38$, what yields $We_u(\Delta = 1) = 9.19$, which lies within the experimental value (Fig. 9a), however, its predicted Δ dependence (as all others) increases faster that observed.

In general, however, the calculations based on the limit of stability of a rotating drop assume that the colliding droplets form a rotating system which smoothly undergoes symmetric breakup as a rotating (equivalent) spherical drop would, with no loss of energy to either internal or vibrational degrees of freedom. This approach has serious limitations. First, symmetric two-droplet outcomes are only observed for $\Delta = 1$ collisions on a limited Weber number range. Second, the initial stages of the collision induce vibrational modes which should also play a roll in determining the outcome. Finally, it is not clear why the loss of energy to non-rotational modes should be negligible. An alternative approach,

which deals with some of these problems was proposed by Ryley and Bennett-Cowell [28] who focused on those energy-damping vibrational modes by proposing that the surface of the temporarily coalesced system oscillates adopting extreme shapes, represented by three model surfaces (Fig. 4 in Ref. 28). When enough energy is available for fragmentation to occur, this is assumed to proceed via the formation of a stretched spherically-ended cylinder (one of the three model shapes) subject to Rayleigh instabilities. However, their theoretical prediction [28] for the rate of energy dissipation is based on parameters (the surface area of each extreme shape and the angular velocity) to be determined experimentally, thus resulting in a model with little predicting power.

One last approach we would like to mention is that of Arkhipov *et al.* [31] who, based on the evolution of the surface shapes, used a variational principle to determine the point in which the effective (surface+rotational) potential between the two droplets losses its attractive minimum. The corresponding prediction is

$$B_u = \frac{1}{\Delta^3}\left[\frac{6(1+\Delta^3)}{We}\right]^{1/2} \tag{7}$$

By setting $B = \Delta = 1$ and solving for We in Eq. (7) one obtains a $We_u(\Delta = 1) = 12$ prediction, 50% higher than the mean experimental value (Fig. 9a). However, against the experimental evidence (Fig. 9b), this theory predicts that We_u should be a rapidly decreasing function Δ.

5.1.4. The effect of "rolling"

We now estimate the effect that the "rolling" motion could have on the upper C-F branch in the present mercury-drop experiments. For simplicity, the calculations will be based on the energy-balance ideas of by Brazier-Smith *et al.* [22] which state that the upper C-F branch reflects the equilibrium between rotational and the surface energies (see Sect. 5.1.2). As mentioned previously (Sect. 3), the "rolling" motion introduces a rotational energy, not always present in collisions between free-moving drops. Since the liquid masses rotate in opposite directions, upon contact the connecting neck is subjected to a "twisting" motion which tends to lower its cohesive strength. We assume that a fraction F of this rolling energy enhances the breaking up of the system. Thus the equilibrium condition now becomes

$$E_{\mathrm{rot}} + FE_{\mathrm{roll}} = \sigma(S_f - S_i), \tag{8}$$

where the left hand side of the equation represent the rotational and the fraction of the rolling energies, and the right hand side, the surface energy change. Using spherical shapes to estimate the moments of inertia, and assuming equal linear momentum for both drops (a good approximation in our experimental situation), the resulting equation for the upper C-F branch is

$$B(We) = \left[\frac{4.8f(\Delta)}{We} - Ff'(\Delta)\right]^{1/2}, \tag{9}$$

with $f(\Delta)$ as defined in Eq. (4) and

$$f'(\Delta) = 0.16\frac{(1+\Delta^3)^{5/3}}{\Delta^3(1+\Delta^2)}.$$

Since, as expected, in the $E_{\rm roll} = 0$ limit, Eq. (9) becomes Eq. (3), we have used its parametric form

$$B(We) = \left[\frac{We_u}{We f(\Delta)} - F f'(\Delta)\right]^{1/2} \tag{10}$$

(leaving F as free parameter), as well as Eq. (4) to fit the data in Figs. 9a and 9b, and the results are shown in Figs. 6a and 6b as solid and dashed curves, respectively. The values obtained using the non-rolling approximation [Eq. (4)] are $We_u = 6.65$, for $\Delta = 1$, and 8.58 for $\Delta = 1.65$, while the corresponding fits, assuming rolling (Eq. 10), yielded $We_u = 8.32$ (with $F = 0.43$) and 11.02 (with $F = 0.75$), *i.e*, approximately 20% higher We_u's than the non-rolling case. Although, given the large fluctuations shown in Fig. 9, both sets of values lie within the systematics reported for free-moving drops, we took the improved overall fit to mercury drop data as justification for using the rolling values shown in Fig. 9a and 9b.

5.2. FRAGMENTATION

The few existing theoretical approaches to fusion-fission type fragmentation can be classified as surface-dynamic and volume-dynamic.

5.2.1. Surface-dynamic model

One example of the surface-dynamic approach is the model of Cârjan, Sierk, and Nix [1], originally developed to simulate nuclear reactions and recently applied to macroscopic drops by us [36]. In this approach the colliding system is represented by a small number (K) of collective degrees of freedom while the internal degrees of freedom are treated implicitly. The shape of the system, assumed to be axially- and reflection-symmetric is described by the Legendre-polynomial expansion

$$\rho_s^2(z) = R_o^2 \sum_{n=0}^{K} q_n P_{2k}(z/z_0), \tag{11}$$

where z is the coordinate along the symmetry axis, ρ_s is the distance perpendicular to the symmetry axis, z_0 is one-half the distance between the two ends of the shape, R_o is the radius of the spherical drop having the mass of the coalesced system, P_{2k} is a Legendre polynomial of degree $2k$, while the q_k's (for $k > 0$) are the K independent symmetric shape coordinates. Assuming incompressibility, the quantity q_0 is determined by volume conservation. The results discussed here are restricted to $K = 5$.

In these calculations, the potential energy of the system is composed of an attractive surface, and a repulsive centrifugal term. The collective kinetic energy is given by

$$T = \tfrac{1}{2} M_{ij}(q)\dot{q}_i\dot{q}_j = \tfrac{1}{2}[M(q)^{-1}]_{ij}\, p_i p_j, \tag{12}$$

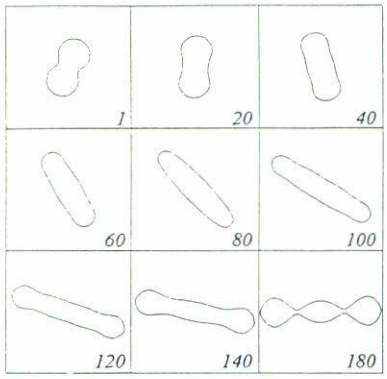

FIGURE 12. Predicted time evolution for a $\Delta = 1$ mercury-drop collision with $B = 0.6$ and $We = 75$, conditions which are similar to those of Fig. 4f. The initial drops move against each other in the horizontal direction, while the time runs as indicated, in units of 1/60 s, twice as fast as the experimental case (Fig. 4f).

where $M_{ij}(q)$ is the shape-dependent inertia tensor. The collective momenta p are related to $\dot{q}$ and M_{ij} through

$$p_i = M_{ij}(q)\dot{q}_j. \tag{13}$$

The internal degrees of freedom are represented by a dissipative force having a mean component in the ith direction:

$$F_i = -\eta_{ij}(q)\dot{q}_j, \tag{14}$$

where $\eta_{ij}(q)$ is the shape-dependent dissipation tensor $\eta(q)$.

With the above ingredients, the generalized Hamilton equations of motion were solved to determine the time evolution of the system. A typical CPU time for one macroscopic drop collision simulation is 10 s in a CRAY YMP computer.

In Fig. 12 we illustrate what is predicted by the dynamical model for a mercury-drop collision having the same initial conditions as the event shown in Fig. 4f. A restriction imposed by the shape parameterization [Eq. (11)] implies that the time evolution predicted by the model begins and ends when the initial and final necks reach a small but finite value, *i.e.*, the simulation starts when the drops are already in contact and stops when the outermost necks reach the limiting diameter. Besides that, and the fact that the real shapes are more complex, the overall features of the observed time sequence seem to be well reproduced by the model: there are three bodies in the final state, and the system separates at a similar angle. There are, however, two important differences: the predicted interaction time is approximately half of what is observed, and the relative size of the drops is less well reproduced, *i.e.*, the model predicts neck-particles which are bigger than the observed ones. The larger mass of the middle drops and the faster time evolution predicted could be expected to result from the assumption of rigid rotation implicit in the model, placing all the available angular momentum in whole-body rotation. Thus the system is predicted to rotate faster and stretch longer.

5.2.2. Volume-dynamic models

The volume-dynamic approach involves the complex task of solving equations of three dimensional unsteady fluid flow with free surfaces. Solutions of the so called Boltzmann-Uhleing-Uhlenbeck and the Landau-Vlasov equations have been very successfull in explaining observables in nuclear reactions [37] and molecular cluster [38] collisions. Unfortunately in these formulations the quantum mechanical aspects are not easily separable from the purely fluid-dynamic ones.

Concerning macroscopic (non-quantal) systems the problem is generally tackled using the finite difference method of solving the Navier-Stokes equations in the bulk. The surface evolution is, then, dealt with in a *ad hoc* way using iterface tracking procedures. One such approach, developed by Lafaurie *et al.* [3], has been used to simulate peripheral and central coalescence drop collisions, resulting in shape evolutions which are very similar to what we observe (compare their Figs. 17 and 18 with our Figs. 4a and 4b). Unfortunately, due in part to the large CPU costs involved (hours and even days per collisions), those hydrodynamic codes have not been used to provide detailed predictions for fragmentation observables (N_p, m_r, etc.). We would like to mention that faster, two-dimensional, simulations by Poo and Ashgriz [39], and Lafaurie *et al.* [3], have been shown to reproduce well the shape evolutions observed in three dimensional liquid drop experiments.

6. CONCLUSION

Collisions of symmetric and asymmetric liquid-drop pairs have been studied experimentally by a number of authors. We reviewed the techniques used in this field concerning drop acceleration, initial and final collision parameter determination. This work includes the techniques developed by our group to cover two different relative velocity regimes, one in which mercury drops of low We are used to study the C-F boundary and the other in which higher We oil drops are used to study multifragmentation. Concerning the mercury-drop experiments, the analysis of 1000 collisions showed that the overall behavior of the resulting data is similar to what has been reported for other liquids, particularly concerning the shape evolution, upper C-F branch, and the limited information available concerning the number and size distributions of the fragments. The higher We oil-drop experiments were used to test recent qualitative theoretical predictions about the formation of so called "exotic shapes." The theoretical situation concerning hydrostatic drop collision models was also given, and the corresponding predictions compared with the available data. The formulations of Brazier-Smith [22] and Schmidt and Lutz [35] were found to provide the best agreement with the upper C-F branch data for $\Delta = 1$ systems, while all models were found to fail in reproducing the weak Δ dependence observed. Concerning fragmentation, a surface-dynamical model, originally developed for nuclear physics, was described, and shown to reproduce some aspects of the observed phenomena.

ACKNOWLEDGMENTS

We acknowledge the financial support of CONACyT Project 4029-E9403.

REFERENCES

1. N. Cârjan, A.J. Sierk, and J.R. Nix, *Nucl. Phys.* **A 452** (1986) 381.
2. L.G. Moretto, K. Tso, N. Colonna, and G.J. Wozniak, *Phys. Rev. Lett.* **69** (1992) 1884.
3. B. Lafaurie, C. Nardone, R. Scardovelli, S. Zaleski, and G. Zanetti, *J. Comp. Phys.* **113** (1994) 134.
4. J. Plateau, *Statistique Expérimentale et Théorique des Liquides soumis aux Seules Forces Moléculaires*, (Gauthier-Villars Publ., Paris., 1873), Vol. 2.
5. Rayleigh, Lord, Further observation upon liquid jets, in continuation of those recorded in the society's proceedings for March and May, 1879, *Proc. R. Soc. London, Ser. A* **34** (1882) 130.
6. *Proceedings of the Third International Colloquium on Drops and Bubbles*, edited by T.G. Wang, Monterrey, Ca., AIP Conf. Proc. **197** (1988).
7. *Proceedings of the Sixth International Conference on Liquid Atomization and Spray Systems*, edited by A.J. Yule and Ch. Dumouchel, Rouen, France (1994).
8. R.A. Park, Ph.D. Thesis, Dept. of Chemical Engineering, U. of Wisconsin, (1970).
9. H.P. Pruppacher and J.D. Klett, *Microphysics of Clouds and Precipitation*, (D. Reidel Publ. Co. Dordrect, Holland, 1978), and references therein.
10. A.M. Podvysotsky and A.A. Shraiber, *Int. J. Multiphase Flow* **10** (1984) 1195.
11. H.T. Ochs III, R.R. Czys, and K.V. Beard, *J. Atmos. Sci.* **43** (1986) 225.
12. N. Ashgriz and P. Givi, *International Journal of Heat and Fluid Flow* **8** (1987) 205.
13. G. Brenn and A. Frohn, *Exp. in Fluids* **7** (1989) 441.
14. N. Ashgriz and J.Y. Poo, *J. Fluid Mech.* **221** (1990) 183.
15. M. Salita, *Journal of Propulsion and Power* **7** (1991) 505.
16. Y.J. Jiang, A. Umemura, and C.K. Law, *J. Fluid Mech.* **234** (1992) 171.
17. A. Menchaca-Rocha, A. Cuevas, M. Chapa, and M. Silva, *Phys. Rev. E* **47** (1993) 1433; A. Cuevas, M. Chapa, M. Silva, and A. Menchaca-Rocha, *Rev. Mex. Fís.* **39** (1993) 428.
18. I.M. Vasenin, V.A. Arkhipov, V.G. Butov, A.A. Glazunov, and V.F. Trofimov, *Gas Dynamics of Two Phase Flow*, (TOMSK University Press, 1986).
19. P.E. Sterninn and A.A. Shraiber, *Multi-phase flow of a gas with particles*, (Publ. Mashinostroerie, Moscow, 1994).
20. A. Menchaca-Rocha, M.E. Brandan, M. Gutiérrez, and R. Labbé, *The Physics Teacher* **24** (1986) 102.
21. J.D. McTaggart-Cowan and R. List, *J. Atmos. Sci.* **32** (1975) 1401.
22. P.R. Brazier-Smith, S.E. Jennings, and J. Latham, *Proc. R. Soc. London, See. A* **326** (1972) 393.
23. R.A. Park and E.J. Crosby, *Chem. Eng. Sci.* **20** (1965) 39.
24. J.Y. Poo and N. Ashgriz, *Exp. in Fluids* **11** (1991) 1.
25. P. Vassallo and N. Ashgriz, *Proc. R. Soc. London Ser. A* **433** (1991) 269.
26. J.R. Adam, N.R. Lindblad, and C.D. Hendricks, *J. Appl. Phys.* **39** (1968) 5173.
27. A. Menchaca-Rocha, *J. Coll. and Int. Sc.* **114** (1992) 472.
28. D.J. Ryley and B.N. Bennett-Cowell, *Int. J. Mech. Sci.* **9** (1967) 817.
29. R. List, C.F. MacNeil, and J.D. McTaggart-Cowan, *J. Geophys. Res.* **75** (1970) 7573.
30. S.G. Bradley and C.D. Stow, *J. Atmos. Sci.* **36** (1979) 495.

31. V.A. Arkhipov, I.M. Vasenin, and V.F. Trofimov, *Zh. Prikl. Mekh. Tekh. Fiz.* **3** (1983) 95.
32. S. Cohen, F. Plasil, and W.J. Swiatecki, *Ann. Phys.* **82** (1974) 557.
33. W.J. Swiatecki, in *Proceedings of the International Colloquium on Drops and Bubbles*, edited by D.J. Collins, M.S. Plesset, and M.M. Saffren (Publ. Jet Propulsion Laboratory, Pasadena CA., 1974), p. 52.
34. J. Blocki and W.J. Swiatecki, *L.B.L. Preprint* 12811-UC-34d (1982).
35. R. Schmidt and H.O. Lutz, *Phys. Rev. A* **45** (1992) 7981.
36. A. Menchaca-Rocha, F. Huidobro, K. Michaelian, A. Pérez, V. Rodriguez, and Cârjan, *Proceedings of the Annual Meeting of the American Chemical Soc.*, Nuclear Chem. Award Symposium, Anaheim, Ca., edited by G. Nebbia and M.N. Namboodiri (World Scientific, Singapore, 1995).
37. J. Aichelin, G. Peilert, A. Bohnet, A. Rosenhauer, H. Stöcker, and W. Greiner, *Nucl. Phys.* **A488** (1988) 437c.
38. M. Guilleumas, F. Gracias, M. Barranco, M. Pi, and E. Suraud., *Z. Phys. D* **25** (1993) 227, and references therein.
39. J.Y. Poo and N. Ashgriz, "Numerical Simulation of Collision of Two-Dimensional Drops," in Proceedings of the 5th Annual Conference on Liquid Atomization and Spray Systems, San Ramon, Ca., (1992) p. 110.